# Dielectric Characterization Of Printed Circuit Substrates

Heyward Riedell, Mike Kay
Real Pomerleau
BNR Inc.
Research Triangle Park, North Carolina

Michael Steer, Jeff Kasten
Mark Basel
Electrical & Computer Engineering
North Carolina State University
Raleigh, North Carolina

## Abstract

The desire to improve high-speed digital signal propagation is the driving force behind research in the area of dielectric characterization. While techniques have been reported for characterizing generic dielectrics, only a few can be applied to printed circuit board substrates. This paper presents a new technique for measuring the dielectric properties of such substrates based on the measured scattering (S) parameters of a transmission line. A discussion of techniques for characterizing the dielectric properties of printed circuit boards is also presented.

## Introduction

The quality of high-speed digital signals is subject to the limitations of the signal transmission network into which components are inserted. As clock speeds continue to increase, circuit designers must be more aware of transmission impairments caused by impedance mismatch, manufacturing tolerances, and transmission line discontinuities. To improve transmission media characterization, techniques to measure the complex permittivity of printed circuit board (PCB) laminates are being investigated. Improved material characterization leads to more accurate circuit simulation during the design phase and tighter control of signal performance after board fabrication.

The most common laminates are fiberglass reinforced resin. Because the composite dielectric is both anisotropic and nonhomogeneous, the electromagnetic field orientation of fabricated planar transmission lines must be preserved in any dielectric characterization test structure. The preservation of field orientation is even more critical considering that multi-layer high-speed composites of such exotic materials as cyanate ester, teflon, and the traditional fiberglass reinforced resin are being proposed. These multilayer structures provide a trade off of the low dielectric constant but high cost of the exotic materials, and the mechanical rigidity, low water absorption and low cost of the fiberglass materials. An additional practical consideration is that existing PCB fabrication processes yield a test coupon (typically 1 cm by 10 cm) for mechanical testing. This coupon could be utilized for substrate characterization of novel composites or for quality assurance of a standard process.

Current substrate characterization techniques generally measure both the real and imaginary part of the complex permittivity. Those suited to laminates can be divided into four major categories; resonance, reflection/transmission, time domain reflectometry (TDR), and phase/length comparison. The new method, based on the measured S-parameters of a transmission line, would be categorized under reflection/transmission methods.

Resonant method calculations of the complex permittivity are based upon the measurement of the resonant frequency and the quality factor for a resonant circuit of some particular geometry. These methods provide information at only a few discrete, harmonically related frequencies specific to the structures involved [1]-[5]. Of the various resonant structures reported only the strip resonators have the same field distribution as planar circuits.

Reflection/transmission methods calculate the permittivity at each frequency sampled and are based upon measured reflection and transmission coefficients [6],[7]. These methods are inherently broadband. Consequently, reflection/transmission methods require less test structures to obtain comparable information than resonant methods. The drawbacks to these methods are the required machining of a dielectric sample and the improper field orientation of the test structure.

TDR methods involve the comparison of the signal reflected from a test device to the incident signal [8]. Fourier analysis is performed converting the time domain response into frequency domain representation. The complex permittivity can be related to the frequency domain reflection coefficient and is found numerically.

The phase/length comparison method compares the electrical and physical length of a pair of transmission lines [9]. The real part of the permittivity is related to the difference in the electrical lengths divided by the difference in the physical lengths. The main drawback, when compared to the other methods previously mentioned,

CH2674-5/89/0000-0102$01.00©1989IEEE

is the inability to determine the imaginary part of the complex permittivity.

Our new method, called parameter transformation, utilizes the S-parameters of a transmission line measured with an automatic network analyzer (ANA). The measurement is de-embedded to remove connector and adaptor errors. The complex permittivity is then calculated by transforming the error corrected S-parameters into impedance parameters and relating them to the transmission line propagation constant.

## Theory

### Definition of Symbols

| | |
|---|---|
| E | Electric Field Intensity |
| H | Magnetic Field Intensity |
| D | Electric Flux Density |
| B | Magnetic Flux Density |
| $\rho$ | Resistivity |
| k | Wavenumber |
| $\omega$ | Radian Frequency |
| $\mu$ | Permeability |
| $\mu_o$ | Free Space Permeability |
| $\gamma$ | Propagation Constant |
| $\varepsilon$ | Complex Permittivity |
| $\varepsilon_o$ | Free Space Permittivity |
| $\varepsilon_r$ | Relative Permittivity |
| $\varepsilon_r'$ | Dielectric Constant |
| $\tan\delta$ | Loss Tangent |
| $V_i^-$ | Voltage Wave scattered from port i |
| $V_i^+$ | Voltage Wave incident on port i |
| $S_{ij}$ | Scattering Parameter associated with ports i and j |
| $V_i$ | Voltage at port i |
| $I_i$ | Current at port i |
| $Z_{ij}$ | Impedance Parameter associated with ports i and j |

### Field Equations and the Complex Permittivity

The solution for the parameter transformation dielectric characterization method falls directly out of the standard wave equations for a generic medium which are derived from Maxwell's equations (1a)-(1d).

$$\nabla \times \mathbf{E} = -\frac{d\mathbf{B}}{dt} \tag{1a}$$

$$\nabla \times \mathbf{H} = \frac{d\mathbf{D}}{dt} + \mathbf{J} \tag{1b}$$

$$\nabla \cdot \mathbf{D} = \rho \tag{1c}$$

$$\nabla \cdot \mathbf{B} = 0 \tag{1d}$$

Assuming that the current density is zero in the medium of interest, the Helmholtz's wave equations (2a and 2b) can be derived in terms of the electric field intensity and the magnetic field intensity. A harmonic time dependence has been assumed in order to simplify the solution. The quantity of interest is the complex permittivity found in the expression for the wavenumber (2c).

$$\nabla^2 E + k^2 E = 0 \tag{2a}$$

$$\nabla^2 H + k^2 H = 0 \tag{2b}$$

$$k^2 = \omega^2 \mu\varepsilon \tag{2c}$$

The propagation constant for transverse electromagnetic (TEM) or quasi-TEM transmission lines, is defined in terms of the wavenumber (3).

$$\gamma = jk = j\omega\sqrt{\mu\varepsilon} \tag{3}$$

If the propagation constant for a transmission line can be found through measurement, the complex permittivity can be calculated directly. Solving equation (3) for the permittivity yields an equation dependent on the propagation constant, radian frequency, and permeability, which is essentially the permeability of free space (4a). The loss tangent is calculated from the real and imaginary parts of the complex permittivity (4b).

$$\varepsilon = \varepsilon_o \varepsilon_r = \varepsilon_o(\varepsilon_r' - j\varepsilon_r'') = -\frac{\gamma^2}{\omega^2 \mu_o} \tag{4a}$$

$$\tan\delta = \frac{\varepsilon_r''}{\varepsilon_r'} \tag{4b}$$

### S-Parameters and Impedance Parameters

The measurements used to solve for the propagation constant and consequently the permittivity are based on the two-port S-parameters of a transmission line. The S-parameters are used to

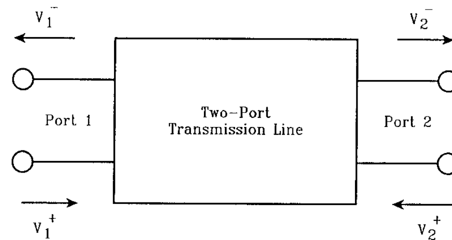


Figure 1: Two-port Scattering Matrix Representation

$$\begin{bmatrix} V_1^- \\ V_2^- \end{bmatrix} = \begin{bmatrix} S_{11} & S_{12} \\ S_{21} & S_{22} \end{bmatrix} \begin{bmatrix} V_1^+ \\ V_2^+ \end{bmatrix} \tag{5}$$

describe high frequency multiport circuits, since voltage and current are nonmeasurable quantities at microwave frequencies. The scattering matrix describes the relationship of travelling voltage waves that are incident and then scattered from each port. In the case of a two-port transmission line section, the scattering matrix is composed of four elements. Figure 1. illustrates the two-port transmission line, and the associated voltage waves are described by equation (5).

An alternative description for a two-port section of transmission line is an impedance matrix. Figure 2. shows the voltages and currents for this representation, and equation (6) defines the relationship of voltage to current.

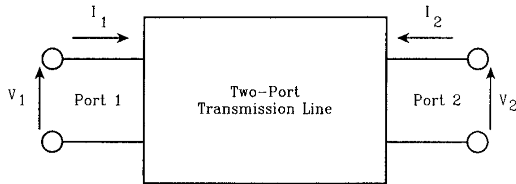


Figure 2: Two-port Impedance Parameter Representation

$$\begin{bmatrix} V_1 \\ V_2 \end{bmatrix} = \begin{bmatrix} Z_{11} & Z_{12} \\ Z_{21} & Z_{22} \end{bmatrix} \begin{bmatrix} I_1 \\ I_2 \end{bmatrix} \quad (6)$$

The elements of the impedance matrix can be used to relate the scattering matrix description of a transmission line to the standard transmission line impedance formula in order to solve for the propagation constant in terms of S-parameters. The transformation from S-parameters to the impedance matrix elements is given in equation (7) and is found in Collin [11].

$$Z_{11} = ((1 + S_{11})(1 - S_{22}) + S_{12}^2)/W \quad (7a)$$

$$Z_{21} = 2S_{12}/W \quad (7b)$$

$$W = (1 - S_{11})(1 - S_{22}) - S_{12}^2 \quad (7c)$$

All that remains is to relate the impedance parameters to the propagation constant. Then the complex permittivity can be calculated directly from measurement.

Relating the Impedance Matrix to the Transmission Line Formula

The transmission line impedance formula (8), as found in Kraus [12], is used to solve for the propagation constant in terms of S-parameters.

$$Z_{in} = \frac{Z_L + Z_c \tanh(\gamma L)}{Z_c + Z_L \tanh(\gamma L)} Z_c \quad (8)$$

If an open circuit is placed at port two, $I_2$ is zero and the $Z_{11}$ element is equal to the input impedance of the transmission line. Thus, the impedance looking into a transmission line with an open circuit at the load is given in equation (9).

$$Z_{11} = \frac{Z_c}{\tanh(\gamma L)} \quad (9)$$

Likewise $Z_{21}$ can be derived by placing a short circuit at port 1. It is assumed that $Z_{11} = Z_{22}$ and $Z_{21} = Z_{12}$ as transmission lines are symmetrical.

$$Z_{21}^2 = Z_{22}^2 - \frac{V_2}{I_2} Z_{22} \quad (10)$$

Now $V_2/I_2$ is the impedance looking into port 2 with a short circuit placed at port one.

$$\frac{V_2}{I_2} = Z_c \tanh(\gamma L) \quad (11)$$

Substituting equations (9) and (11) into equation (10) gives $Z_{21}$ in terms of the propagation constant and the characteristic impedance.

$$Z_{21} = Z_c \operatorname{csch}(\gamma L) \quad (12)$$

Finally, by utilizing equations (7), (9) and (12) the propagation constant is expressed in terms of S-parameters.

$$\gamma = \frac{1}{L} \left( Ln \sqrt{A + A^2 - 1} \right) \quad (13a)$$

$$A = \frac{(1 + S_{11})(1 + S_{22}) + S_{12}^2}{2S_{21}} \quad (13b)$$

Equation (13) is substituted into equation (4) to solve for the complex permittivity in terms of S-parameters.

Test Procedure

The equipment setup for the parameter transformation method is shown in Figure 3. A

Hewlett Packard 8510 ANA was used to measure the two-port S-parameters of a planar transmission line fabricated on a stripline PCB. A semi-rigid coaxial cable with a characteristic impedance of 50 ohms connected the ANA to two 3.5 mm subminiature A (SMA) connectors. These SMA connectors were in turn soldered to the PCB.

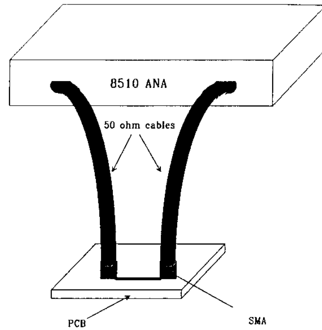


Figure 3: Equipment Setup

The S-parameters provided by the ANA contain adaptor errors introduced by the connection between the coaxial cables and the actual PCB transmission line. These errors were de-embedded to produce an S-parameter description of only the two-port transmission line [10]. At this point the data was processed into the dielectric constant and loss tangent utilizing the impedance parameter transformation and its relationship to the propagation constant.

| Legend | | |
|---|---|---|
| (a) | O | Parameter Transformation |
| (b) | □ | Coax Reflection |
| (c) | Δ | Strip Resonance |

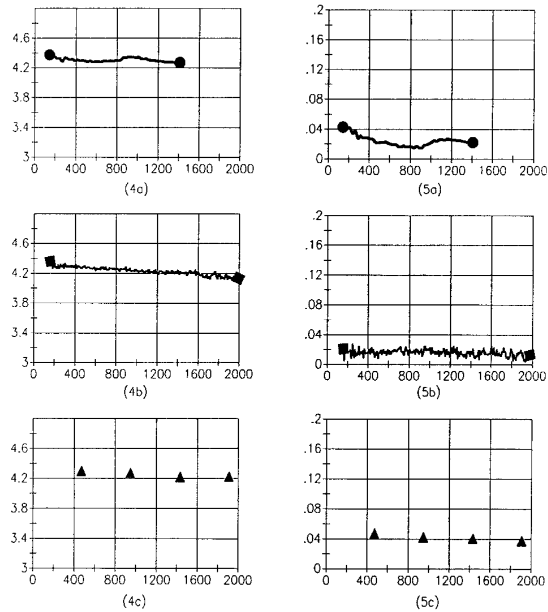


Figures 4a, b, c: Dielectric Constant as a function of frequency (Mhz)

Figures 5a, b, c: Loss Tangent as a function of frequency (Mhz)

## Results

The parameter transformation technique was compared with the two previously published methods of strip resonance [1]-[5] and coaxial reflection [6],[7]. Measurements for each method were performed on a resin material reinforced with fiberglass (FR4). Figures 4 and 5 illustrate the dielectric constant and loss tangent calculated for the three techniques. The resonant technique produces discrete results and is plotted as such. The other two methods are broadband techniques and are plotted as continuous functions of frequency.

## Discussion

The results in Figures 4. and 5. indicate that all three methods compare favorably in the calculation of a dielectric constant of about 4.3. Both the parameter transformation method and the coaxial reflection technique have a slightly lower calculation of the loss tangent (.02 - .03) than does the resonant method (.04). This deviation is to be expected for the coaxial technique, since it only provides accurate information for loss tangents with values greater than 0.1 [6].

The accuracy of the parameter transformation method is affected by the numerical precision of the measured data. Application of this technique to several S-parameter data sets generated with a microwave simulator showed reduced performance in regions where the magnitude of $S_{11}$ approached a minimum. In addition, some measured data sets produced results with considerable jitter about an average value that followed the trend in figures 4a and 4b. These regions of uncertainty do not impede interpretation of the final results since the dielectric constant and loss tangent are well behaved with frequency for this FR4 test sample.

## Conclusion

We have found that the parameter transformation technique has several advantages over other dielectric characterization methods. Our technique is based upon measurements with the same electric and magnetic field distributions as a printed circuit trace.

This attribute should lead to more accurate values for anisotropic, nonhomogeneous materials such as the composite substrates being explored for high-speed digital signal propagation. Of all the other techniques, only the strip resonator and phase/length comparison methods generate the same field patterns. However, both of these require much more space to generate comparable information, and the resonant technique is not broadband. Our test structure is as simple to fabricate as an ordinary PCB trace. Other methods require the machining of samples and/or several error minimizing attempts before results are forthcoming. Our technique's results compare favorably with two established techniques for homogeneous dielectrics. Finally, our approach can be utilized with test coupons for the testing of novel dielectric composites or for quality assurance purposes. None of the other procedures are both broadband and small enough for coupon testing. These attributes make the parameter transformation technique an appealing method of high-speed printed circuit dielectric characterization.

## References


[1] Olyphant Jr., M. "Microwave Substrates Support MIC Technology," Microwaves, pp. 47-52, December 1980.

[2] Olyphant Jr., M.,. and Ball, J. H. "Strip-Line Methods for Dielectric Measurements at Microwave Frequencies," IEEE Transactions of Electrical Insulation, Vol. EI-5, NO. 1, pp. 26-32, March 1970.

[3] Edwards, T. C., and Owens, R. P. "2-18 GHz Dispersion Measurements on 10-100 Ohm Microstrip Lines on Sapphire," IEEE Transactions on Microwave Theory and Techniques, Vol. MTT-24, No. 8, pp. 506-513, August 1976.

[4] Deibele, S., and Beyer, J. B. "Measurements of Microstrip Effective Relative Permittivities," IEEE Transactions on Microwave Theory and Techniques, Vol. MTT-35, NO. 5, pp.535-538, May 1987.

[5] Hubbell, S., and Angelakos, D. J. "A Technique for Measuring the Effective Dielectric Constant of a Microstrip Line," IEEE Transactions on Microwave Theory and Techniques, Vol. MTT-31,No. 8, pp. 687-688, August 1983.

[6] Tashiro,S. "Measuring the Dielectric Constant of Solids with the HP 8510 Network Analyzer," Product Note 8510-3, Hewlett-Packard Instrumentation Company, August 1985.

[7] Barry,W. "A Broad-Band, Automated, Stripline Technique for the Simultaneous Measurement of Complex Permittivity and Permeability," IEEE Transactions on Microwave Theory and Techniques, Vol. MTT-34, No. 1, pp. 80-84, January 1986.

[8] Boned, C., and Peyrelasse, J. "Automatic Measurement of Complex Permittivity (from 2 MHz to 8 GHz) Using Time Domain Spectroscopy," J. Phys. E., Vol 15, No. 5, pp. 534-538, May 1982.

[9] Das,N. K., Voda, S. M., and . Pozar, D. M. "Two Methods for the Measurement of Substrate Dielectric Constant," IEEE Transactions on Microwave Theory and Techniques, Vol. MTT-35,No7, pp.636-641, July 1987.

[10] Kasten, Jeffrey S., Steer, M., and Pomerleau, R. "Through Symmetric Fixture: A Two-port S-parameter Calibration Technique", Proceedings RF Expo East 88, Philadelphia, Penn., Cardiff Publishing Co., pp. 367-380, Oct. 1988.

[11] Collin, R. E. Foundations for Microwave Engineering, McGraw-Hill, Inc., New York, NY, 1966,p. 201.

[12] Kraus, John D. Electromagnetics, McGraw-Hill, Inc., New York, NY,1984, p. 404.

Session 10B7

# Microstrip Discontinuity Modeling

Glen Stewart, Michael Kay
Heyward Riedell, Real Pomerleau
BNR Inc.
Research Triangle Park, North Carolina

Michael Steer
Electrical & Computer Engineering
North Carolina State University
Raleigh, North Carolina

## Abstract

In this report we develop an efficient modeling technique for microstrip discontinuities. The technique obtains closed form expressions for the lumped element equivalent circuits which are used to model these discontinuities.

To describe our technique, we focus on the bend discontinuity and report the inductance, and capacitance of the equivalent circuit as calculated by an expression developed with this technique.

## Introduction

### Definition of problem

Due to layout necessities, an electromagnetic wave that propagates down a microstrip line may encounter discontinuities such as bends, tees, and vias. These discontinuities cause disturbances in the electric and magnetic fields which affect the integrity of the signal. It is the prediction and control of the these disturbances that face the Printed Circuit Board (PCB) designer and have made CAD capabilities essential to the engineering process. Engineers must be able to simulate and test their printed circuit designs before major expenses are committed to PCB construction. In order for the CAD process to be an interactive one, the calculation of the circuit characteristics must be relatively fast. Also, the accuracy of these calculations is equally important since realistic simulations are essential.

In general, models for the transmission line effects of microstrip transmissions lines have been both fast and relatively accurate. However, most models of microstrip discontinuities are numerically cumbersome or do not maintain accuracy as frequency increases. Therefore, the heart of the simulation problem is to develop discontinuity models that are numerically efficient and maintain reliability even at relatively high frequencies.

## Background

Many papers have addressed the modeling of microstrip discontinuities in terms of lumped element equivalent circuits. In these circuits the disturbances in the electric and magnetic fields are represented as an equivalent capacitance and an equivalent inductance respectively. In the past a quasi-static approach has been used to arrive at values for these equivalent capacitances and inductances [6]; however, there are several disadvantages to this method.

One disadvantage in quasi-static techniques is that extensive computation times are often required to arrive at a value for the desired parameter. As indicated by Anders and Arndt, in their report on the moment method, it can take several minutes per data point to calculate the capacitances and inductances of some discontinuities [1]. Similar computation times are also reported for the matrix inversion method [3]. With these long computation times an interactive design session could not be realized.

Another problem that exists with quasi-static methods is that they cannot take into account the higher order modes, and as a result, they begin to show errors at high frequencies. To solve this problem, many have turned to the planar waveguide model, presented in [4], to assist in the calculations of the scattering (S) parameters, of several discontinuities. These calculated S-parameters have been shown to maintain reasonable accuracy up to approximately 12 GHz.

## Approach

Sylvester and Benedek pointed out that the problems of computation time in their technique could be overcome by fitting empirical equations to the curves which the technique generates [2]. The resulting expressions are faster, but their accuracy depends on the accuracy of the original results. If an accepted level of accuracy exists for the original data, a reliable expression can be developed to represent the data. Our approach is to depend on measurements to give us a collection of accurate data and the use of curve-fitting techniques to obtain empirical expressions to represent the data.

CH2674-5/89/0000-0107$01.00©1989IEEE

We are focusing this paper on a bend discontinuity where the angle of the bend is allowed to vary from 22.5 to 90 degrees. Although other physical parameters, such as the width of the trace, the dielectric constant, and the thickness of the dielectric, are important to the characteristics of the bend, only the angle of the bend will be allowed to vary. However, the techniques of curve-fitting can be applied to include all of the important physical parameters. The only reason for limiting the number of variables is to simplify the presentation of the technique. As a result, the final closed form equation will be a function of only frequency and the angle of the bend.

## Theory

### Definitions

Several network parameters are used by this technique. We begin with measured S-parameters and use T-parameters and Z-parameters during the development of the models. All of these parameters represent certain characteristics of a network.

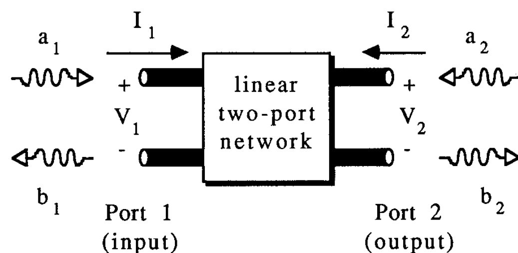


Figure 1: A linear two-port network and its associated input and output quantities.

Figure 1 shows a two-port network with both the input and output parameters displayed. From this network the S-parameters are obtained as follows:

$$b_1 = S_{11}(a1) + S_{12}(a2)$$
$$b_2 = S_{21}(a1) + S_{22}(a2) \qquad (1)$$

where a and b are the incident and reflected waves of the network. These equations can be represented in matrix form as

$$\begin{bmatrix} b_1 \\ b_2 \end{bmatrix} = \begin{bmatrix} S_{11} & S_{12} \\ S_{21} & S_{22} \end{bmatrix} \begin{bmatrix} a_1 \\ a_2 \end{bmatrix}. \qquad (2)$$

The S-parameters give us a way of representing a network's transmission and reflection coefficients, and they are the only parameters that can be measured at high frequencies. They are, however, non-cascadable. When we need to consider a cascade of S-parameters we must convert them to T-parameters according to the conversion expressions given in [7] and summarized in Table 1. In fact, the T-parameters are sometimes refered to as cascadable S-parameters

Table 1: [S] ¤ [T] Conversions

| [S] to [T] | [T] to [S] |
|---|---|
| $t_{11} = \dfrac{1}{s_{21}}$ | $s_{11} = \dfrac{t_{21}}{t_{11}}$ |
| $t_{12} = -\dfrac{s_{22}}{s_{21}}$ | $s_{12} = t_{22} - \dfrac{t_{21}t_{12}}{t_{11}}$ |
| $t_{21} = \dfrac{s_{11}}{s_{21}}$ | $s_{21} = \dfrac{1}{t_{11}}$ |
| $t_{22} = s_{12} - \dfrac{s_{11}s_{22}}{s_{21}}$ | $s_{22} = -\dfrac{t_{12}}{t_{11}}$ |

Table 2: [S], [Z] Conversions

$$z'_{11} = \frac{(1+s_{11})(1-s_{22})+s_{12}s_{21}}{\Delta_2} \qquad z'_{12} = \frac{2\,s_{12}}{\Delta_2}$$

$$z'_{22} = \frac{(1-s_{11})(1+s_{22})+s_{12}s_{21}}{\Delta_2} \qquad z'_{21} = \frac{2\,s_{21}}{\Delta_2}$$

$$s_{11} = \frac{(z'_{11}-1)(z'_{22}+1)-z'_{12}z'_{21}}{\Delta_1} \qquad s_{12} = \frac{2\,z'_{12}}{\Delta_1}$$

$$s_{22} = \frac{(z'_{11}+1)(z'_{22}-1)-z'_{12}z'_{21}}{\Delta_1} \qquad s_{21} = \frac{2\,z'_{21}}{\Delta_1}$$

$$\Delta_1 = (z'_{11}+1)(z'_{22}+1) - z'_{12}z'_{21}$$
$$\Delta_2 = (1 - s_{11})(1 - s_{22}) - s_{12}s_{21}$$
$$z'_{11} = z_{11}/Z_o \; ; \; z'_{12} = z_{12}/Z_o \; ;$$
$$z'_{21} = z_{21}/Z_o \; ; \; z'_{22} = z_{22}/Z_o \; ;$$

The Z-parameters represent the impedance characteristics of a network. Their development is similiar to that of the S-parameters and conversions

between Z-parameters and S-parameters are accomplished through the use of the conversion expressions of Table 2 [7]. The Z-parameters are represented in matrix form as follows:

$$\begin{bmatrix} V_1 \\ V_2 \end{bmatrix} = \begin{bmatrix} Z_{11} & Z_{12} \\ Z_{21} & Z_{22} \end{bmatrix} \begin{bmatrix} I_1 \\ I_2 \end{bmatrix} \tag{3}$$

where

$$V_1 = a_1 + b_1$$

$$V_2 = a_2 + b_2 \tag{4}$$

with $I_1$ and $I_2$ being the corresponding currents.

Removing Unwanted Effects by De-embedding and Stripping

Figure 2a shows the coax-to-microstrip test fixture we used while developing our expressions. The test fixture consists of five sub-structures; two connectors, two lengths of line that the connectors are attached to, and a "point discontinuity" where we used the concept of a point discontinuity to describe the perturbations in the fields due to the effects of the discontinuity. Each sub-structure of this fixture has its own characteristics and can be represented by a set of S-parameters (Figure 2b). To isolate the characteristics of the bend, the effects of all the sub-structures must be removed. The de-embedding techniques outlined in [5] can be used to remove the effects of the connectors. We developed a method for removing the effects of the lengths of line that link the connectors to the bend.

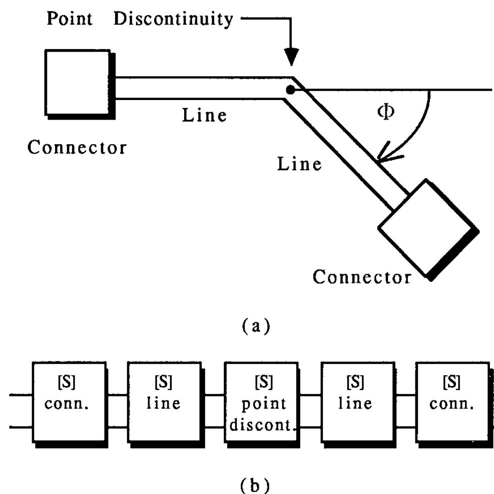


Figure 2 a) Test fixture for the bend discontinuity
b) Sub-structures represented by S-parameters.

After the de-embedding is performed, we strip the remaining structure of the effects of the microstrip lines on either side of the discontinuity, by a method of vector multiplication on a T-parameter network. By de-embedding the test fixture of Figure 2a, we were left with a set of S-parameters that represent the two lengths of line, and the point discontinuity (see Figure 3). From these S-parameters we obtained a cascade of T-parameters according to the conversion expressions summarized in Table 1. These T-parameters are represented mathematically as

$$[T_{tot}] = [T_{l1}][T_{pd}][T_{l2}] \tag{6}$$

where $[T_{l1}]$ and $[T_{l2}]$ are the T matrices of the lines, and $[T_{pd}]$ is the T matrix of the point discontinuity.

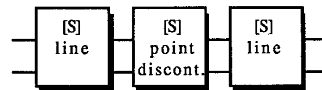


Figure 3: S-parameter representation of test fixture after de-embedding.

In order to obtain the T-parameters of the point discontinuity from Equation 6, we first needed to find the T-parameters of the lines. A test structure similar to that of Figure 2a was used for this purpose. The bend was removed from the structure leaving a straight microstrip line of known length. The S-parameters of the length of line were measured, and de-embedding was performed to remove the effects of the connectors. The result was a set of S-parameters that represented only the line. Again the conversions of Table 1 were used to convert to T-parameters.

The only quantity in Equation 6 remaining unknown to us at this point was the T-parameters of the point discontinuity. Equation 6 was solved for these parameters to give

$$[T_{pd}] = [T_{l1}]^{-1}[T_{tot}][T_{l2}]^{-1}. \tag{7}$$

Bend Equivalent Circuit

The equivalent circuit that was used by Gupta [6] for the 90 degree bend is shown in Figure 4a. This circuit can be expanded by using impedance and admittance elements, as shown in Figure 4b, instead of only capacitors and inductors. It is shown in [8] that if the network is assumed to be symmetric, the impedance elements of a two-port tee network can be represented as follows:

$$Z_a = Z_{11} - Z_{12}$$

$$Z_b = Z_{22} - Z_{12} \tag{8}$$

$$Y_c = 1/Z_{12} \quad .$$

The values of the impedances of Figure 4b can be obtained, according to Equations 8, after the Z-parameter representation of the network is determined. The Z-parameters are obtained from measured S-parameters by using the conversion expressions of Table 2.

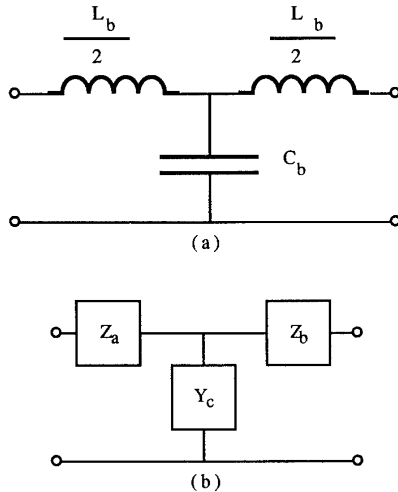


Figure 4 a) Equivalent circuit for a 90 degree bend.
b)Enhanced equivalent circuit.

## Curve Fitting Technique

If an accurate set of Z-parameters is available, curve-fitting techniques can be used to arrive at expressions for the impedances of Figure 4b. Many procedures are available for fitting empirical expressions to measured data. Among these are multi-dimensional regression for the development of polynomial fits, and fits which are based on physically justified functionals such as tanh(x). The first allows for interpolation between data points, and functional fits supply a means for obtaining extrapolation capabilities.

In [9] we find many solutions to the problems of curve-fitting. The approach taken by most curve-fitting techniques is to define a function ("merit function" [9]) which will decrease as the agreement between the measured data, and an empirical equation, increases. The goal then is to minimize the merit function. This source, [9], discusses the choice of a merit function, techniques by which the merit function can be minimized, and several approaches for dealing with both linear and non-linear data.

## Method

In order to address the angle at which the bend occurs, we considered four structures covering four different bend angles; 22.5, 45, 67.5, and 90 degrees. The S-parameters for each of these structures were measured with a Hewlett-Packard 8510B Automatic Network Analyzer (ANA).

The set of measured S-parameters was then submitted to the de-embedding process where the effects of the connectors were removed. Next, the effects of the lines were removed by the stripping method, according to Equation 7. We were then left with a set of S-parameters that represented the effect of the point discontinuity alone.

For the purposes of this report the equivalent circuit of Figure 4b was used to represent the bend discontinuity. The S-parameters of the point discontinuity were converted to Z-parameters (Table 2), and these Z-parameters were used to obtain the values of $Z_a$, $Z_b$, and $Y_c$ of Figure 4b. The imaginary parts, or reactances, of $Z_a$, $Z_b$, and $Y_c$ were then used to obtain values for the inductances and capacitance of Figure 4a. Finally, the curve-fitting techniques were applied to the values of $L_b$, and $C_b$, to develop general closed form expressions for both.

## Results

We developed a general expression for the lumped elements of Figure 4a. These expressions are a function of frequency and the angle of the bend, and are valid for bends from 22.5 to 90 degrees. Figure 5 shows the values of capacitance and inductance for a 45 degree bend as calculated by the expressions we've developed.

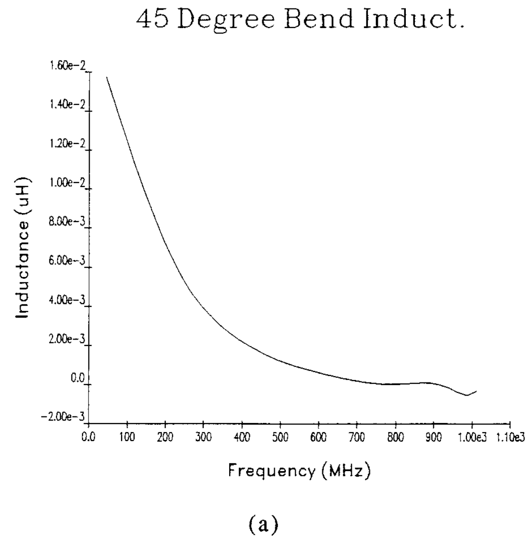


(a)

45 Degree Bend Cap.

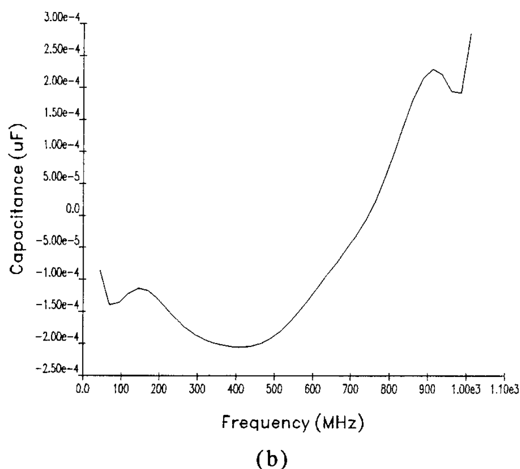


Figure 5: a) Calculated Inductance for a 45 degree bend.
b) Calculated Capacitance for a 45 degree bend.

## Conclusion

We have described a technique by which fast and accurate expressions can be obtained for the lumped elements of equivalent circuits for microstrip bends. It is based on fitting measured data to empirical expressions. It can be applied to any microstrip discontinuity, and if enough data is available for the curve fitting techniques to properly characterize the discontinuity, all the important parameters can be considered.

## References

[1] Anders, Peter, and Arndt, Fritz."Microstrip Discontinuity Capacitances and Inductances for Double Steps, Mitered Bends with Arbitrary Angle, and Asymmetric Right-Angle Bends," IEEE Trans.on Microwave Theory and Techniques, Vol,. MTT-28, pp. 1213-1217, Nov. 1980.

[2] Sylvester, P., and Benedek, P. "Equivalent capacitances of microstrip open circuits," IEEE Trans. Microwave Theory and Tech.,Vol. MTT-20, pp. 511-516, Aug. 1972.

[3] Farrar, Andrew, and Adams, Arlon Taylor. "Matrix Method for Microstrip Three-Dimensional Problems," IEEE Trans. on Microwave Theory and Tech., vol.MTT-20, pp. 497-504, Aug. 1972.

[4] Kompa, G., and Mehran, R. "Planar Wavequide Model for Calculating Microstrip Components," Electron. Lett., Vol. 11, pp. 458-460, Sept. 1975.

[5] Kasten, Jeffery S., Steer, Michael, and Pomerleau, Real "Through Symmetric Fixture: A Two-port S-parameter Calibration Technique," Proceedings RF Expo East 88, Philadelphia, Penn., Cardiff Publishing Co., pp. 367-380, Oct. 1988.

[6] Gupta, K.C., Garg, Ramesh, and Chadha, Rakesh, "Computer Aided Design of Microwave Circuits," Norwood, Mass: Artech House, 1981.

[7] Gonzalez, Guillermo, "Microwave Transistor Amplifiers," Prentice-Hall, Inc., Englewood Cliffs, NJ, pp.24-25, 1984.

[8] Collins, Robert E., "Foundations for Microwave Engineering," McGraw-Hill Book Company, New York, NY, 1966.

[9] Press, William H., Flannery, Brian P., Teukolsky, Saul A., and William T. Vetterling, "Numerical Recipes," Cambridge University Press, New York NY, 1986.

GLEN STEWART

Glen Stewart graduated from North Carolina State University in 1988 with a Bachelor of Science in Electrical Engineering. Since graduating he has been working as a co-op engineer at BNR while he attends graduate classes at North Carolina State University. At BNR he has been studying the affects that various discontinuities have on the transmission of signals over printed circuit boards. He will return to graduate school full time in the fall and will complete the requirements for his Masters of Science in Electrical Engineering in the spring of 1990.

MICHAEL KAY

Michael Kay graduated from the University of Florida in 1987 with a Bachelor of Science in Electrical Engineering. During his undergraduate studies, he worked several co-op terms at Honeywell Inc. in Clearwater Florida working with laser navigation and IC design. Michael will complete his Master of Science in Electrical and Computer Engineering at North Carolina State University in May, 1989, specializing in analog circuit design. He is presently working his third co-op term at BNR Inc. studying high speed printed circuit boards while finishing school.

C. Heyward Riedell

Heyward Riedell received his Batchellor of Science in Electrical Engineering from N.C. State University in 1986. During his undergraduate study he worked part time for the Microelectronics Center for North Carolina studying spin coating polymers for electrical insulation purposes on integrated circuit substrates. Since 1987, he has been employed with BNR as a research engineer studying high frequency characteristics associated with printed circuit boards. Heyward will receive his Master of Science in Electrical Engineering from N.C. State University in May of 1989.

# Empirical Statistical Analysis Of Planar Transmission Lines On PCBs Accounting For Manufacturing Variations

Michael Kay, Real Pomerleau
BNR Inc.
Research Triangle Park, North Carolina

Michael Steer
Electrical & Computer Engineering
North Carolina State University
Raleigh, North Carolina

## Abstract

The effect of random process variations in Printed Circuit Board (PCB) manufacturing with controlled impedance can cause significant deviation from design intent. This paper will describe an empirical analysis which quantitatively describes the repeatability of a particular process of microstrip manufacturing. It will also address the problem of random manufacturing variations in PCB structures.

## Introduction

The transmission line effects between high speed digital devices on a PCB is becoming a more significant design issue as the speed and size of processors and systems increase. Theoretical models and simulators have been created to predict the PCB transmission line effects, but little has been done to model the random impedance variations resulting from a manufacturing process. This paper addresses the problem of random manufacturing variations in PCB structures as well as describes an empirical technique to perform a statistical analysis of PCB lines. The technique will improve transmission line characterization by enabling a worst case analysis of transmission line effects to be done. This will allow the designer to minimize post-prototype problems associated with high speed PCBs concerning inconsistencies in a manufacturing process.

The description of PCB structures is obtained by measuring the Scattering (S) parameters and then converting them to frequency domain characteristic impedance (Z0) and propagation constant (gamma). A deviation in complex Z0 and gamma can be used to model line and discontinuity variations.

With the use of this technique, a better representation of Z0 and gamma can be obtained than by previous techniques. Presently, the most popular way to calculate Z0 and gamma is through the use of time domain reflectometry (TDR). TDR involves the use of an oscilloscope, and measuring intermediate voltages in the propagation of a step function through a transmission line. However, this process is subject to several significant errors:

1) The reflection caused by the connectors is not taken into consideration
2) Shunt and series losses also introduce uncompensated error to the TDR measurement
3) Z0 and gamma are only given as a constant instead of as a function of frequency.

In response to these errors, the technique described in this paper removes the effects of the connectors, characterizes loss, and returns impedance and gamma as a function of frequency, resulting in a much more accurate model than before.

## Theory

A description of S-parameters is necessary to understand the basis of this analysis. S-parameters are used instead of a voltage and current parameter because the S-parameters describe the relative amplitude and phase of

CH2674-5/89/0000-0112$01.00©1989IEEE

forward and backward traveling waves. Because we measure transmission line effects of up to 10 GHz (in this paper) microwave measurement techniques must be used. Therefore, S-parameters are useful because they are directly measurable at these frequencies. Figure 1 describes how S-parameters are defined in a two-port network.

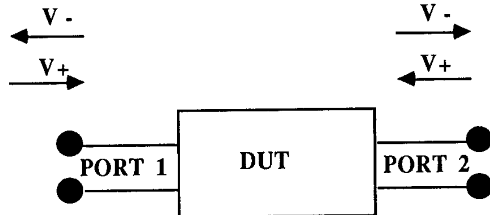


Figure 1: Description of Two-port S-parameters

V+ = Forward traveling wave (applied)
V- = Backward traveling wave (measured)

$V1- = (S_{11} * V_1+) + (S_{12} * V_2+)$
$V2- = (S_{21} * V_1+) + (S_{22} * V_2+)$

The automatic network analyzer (ANA) has two ports and returns four complex S-parameters for each frequency point. $S_{11}$ is the port one reflection coefficient which describes the relative amplitude of the signal reflected back to port one as a function of frequency after a signal is applied. $S_{11} = V_1-/V_1+$ when port two is matched. $S_{21}$ is the port one transmission coefficient, which describes the relative amplitude of signal that is transmitted from port one through to port two ($S_{21} = V_2-/V_1+$). $S_{12}$ and $S_{22}$ are measured the same way from port two. A magnitude and phase term is given for with each S-parameter.

The S-parameters of a straight line on a microstrip PCB are dependent mainly on four parameters of the board as shown in Figure 2.

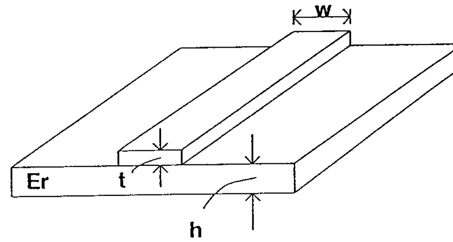


Figure 2: Microstrip board parameters.

W = Width of PCB line
T = Thickness of PCB line
H = Width of dielectric material (distance between line and ground plane)
Er= Dielectric constant of material

Each of the board parameters affect impedance differently. The actual amount that Z0 and gamma varies depends on which parameter is being considered.

Though S-parameters are a good way to measure a line, they are not the best way to describe it physically. A more intuitive description of a PCB line is obtained from the characteristic impedance and the propagation constant of the line which can be calculated from the S-parameters. Equations 1 and 2 were used to calculate Z0 and gamma from the S parameters (see reference [1] for derivation). Z0 is described in magnitude phase form and is independent of board length. Gamma contains a real and imaginary part. The real part, alpha, is the attenuation constant and the imaginary part, beta, is the phase constant, both of which are functions of line length. $Z_m$ is the impedance to which the board was intended to be manufactured (50 ohms).

$$Zo = \frac{-b - \sqrt{b - 4ac}}{2a} \tag{1}$$

$$a = (S_{11} - 1 - S_{11}S_{22} + S_{12}S_{21} + S_{22})$$

$$b = (2 \times Z_m)(S_{11} - S_{22})$$

$$c = Z_m^2(S_{11} + 1 + S_{11} S_{22} - S_{12} S_{21} + S_{22})$$

$$Gamma = \left(\frac{1}{Length}\right) \ln\left[A + \sqrt{A - 1}\right]$$

$$A = \left[\frac{(1 + S_{11})(1 - S_{22}) + S_{12} S_{21}}{2 S_{21}}\right] \tag{2}$$

Since S-parameters are complex numbers, taking the square root causes phase discontinuity problems when implementing Equations 1 and 2 using Fortran 77. The problem occurs when the parameter passes through the negative real axis of the complex plane. For this reason, it is necessary to keep track of the absolute phase of each variable, instead of just considering it from -180 to +180 degrees.

In order to obtain a statistical description of Z0 and Gamma, in this paper, repeated S-parameter measurements were made of identical structures. These measurements were then converted to Z0 and Gamma. Then the mean and standard deviation were calculated as a function of frequency using Equations 3 and 4. The standard deviation describes the repeatability of manufacturing and measuring the line.

$$\overline{X} = \text{MEAN} = \frac{1}{N}\sum_{i=1}^{N} X_i \qquad (3)$$

$$\text{STANDARD DEVIATION} = \sqrt{\frac{1}{N}\sum_{i=1}^{N} (X_i - \overline{X})^2} \qquad (4)$$

In order to address the problem of manufacturing variation, the inherent variation of the test setup needs to be characterized. This setup consists of an HP 8510 network analyzer with precision 3.5 mm connectors. These connectors are attached to a microstrip-to-SMA adapter which is soldered to the PCB. Figure 3 shows the test setup.

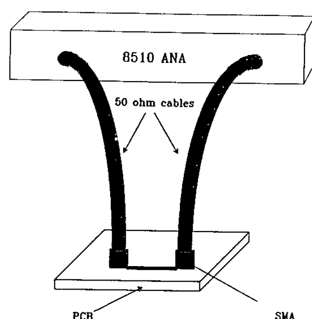


Figure 3: Test Setup

The repeatability of the connection between the precision 3.5mm connector and the microstrip-to-SMA adapter is then determined. Next we determine the repeatability of the connection of the adapter to the PCB involving solder joints that bonded two adapters to the test board.

Removing the errors caused by the measurement process will give us the manufacturing deviation only. When adding several random variables, the deviation of the sum is simply the square root of the sum of the deviations. Since soldering the SMA adapters to the PCB takes into account the variation caused by both the soldering of the SMAs and the connecting of the ANA cable, only this effect needs to be subtracted from the deviation caused by sampling different lines. Equation 5 gives the standard deviation of just the random manufacturing variations.

$$SD_3 = \sqrt{SD_2^2 - SD_1^2} \qquad (5)$$

$SD_1$ = standard deviation caused by measuring process
$SD_2$ = sta. dev. caused by measuring and manufacturing process
$SD_3$ = sta. dev. caused by just the manufacturing process

## Method

This paper presents a method to empirically describe the manufacturing variations of a PCB structure. An eight mil microstrip line was chosen for the testing and was manufactured on a controlled impedance test board. The board impedance was manufactured to an intended impedance of 50 ohms based on existing formulas for the physical dimensions and manufacturing process. We measured a total of 20 microstrip lines on 10 separate test boards.

To measure the structures on these boards, the following equipment was used:

- An HP 8510 Network Analyzer, which produces an S-parameter matrix as a function of frequency
- Microstrip-to-SMA adapters soldered to the test boards
- A torque wrench to connect the coax

cable coming from the ANA to the SMA adapters.

For all measurements, we set the following parameters on the HP8510B:

- A frequency range of 45 MHz to 10 GHz
- 801 frequency points per measurement
- Power of 10 dBm
- 16 separate measurements were averaged in the ANA before storing them. Averaging improves dynamic range by reducing the effect of individual measurement deviations. Noise on an individual measurement is reduced by 20log(1/N) dB where, in this case N, is 16.

The description of the random deviation caused by just the manufacturing inconsistencies is made by:

1) Measuring all 20 structures and determining the variations about a mean
2) Choosing one structure to determine the variations of making connections from the ANA to the SMA adapter
3) Choosing one structure to determine the variations of soldering SMA adapters to PCBs
4) Removing the random deviation caused by the measurement process (2 and 3) from the measured deviation of all the structures (1). This is done by a process described in reference [3] called the "total sum of squares of deviations."

The ANA measures the S-parameters of the cables, connectors, and PCB structures, even though all we want is the effects of the structures. Therefore, the effects of the cables and connectors must be mathematically removed. The process of removing the effects of the cables is called calibration and in done within the ANA before the data is sent to the PC to be further analyzed and stored. The process of removing the effects of the connectors is called de-embedding which utilizes techniques described in reference [2]. After both of these processes are complete, we are left with S-parameters representing only the PCB structure.

Since S-parameters are not a particularly convenient way to model a PCB line or analyze it statistically, and Z0 and gamma are used to model PCB lines and discontinuities in the transmission line simulator being developed at NCSU, the conversion from S-parameters to Z0 and gamma is necessary. This is done by means of Equations 1 and 2.

The mean and standard deviation of Z0 and gamma is generated as a function of frequency, and a routine is written to collect the data and calculate these numbers. The standard deviation describes the repeatability of a measurement.

The deviation of just the manufacturing variations must be extracted from the additional random effects added by the measurement technique. This is accomplished by an analysis of variance technique called "the total sum of squares of deviations" described in reference [3] and given by Equation 5. This result is used to create statistical models which are implemented in a transmission line simulator to do a worst case analysis of the random effects of the PCB on signal propagation.

## Results

The results describe, as a function of frequency, the repeatability (standard deviation) of the different errors encountered in the measurement and manufacturing process :

1) Connecting ANA cables to SMA adapters on a PCB using a torque wrench (connecting deviation only)
2) Soldering SMA adapters to a PCB (includes: soldering deviation plus connecting deviation)
3) Total measurement (includes: boards deviation, soldering deviations, plus connecting deviation)
4) Manufacturing a PCB line (board deviation only).

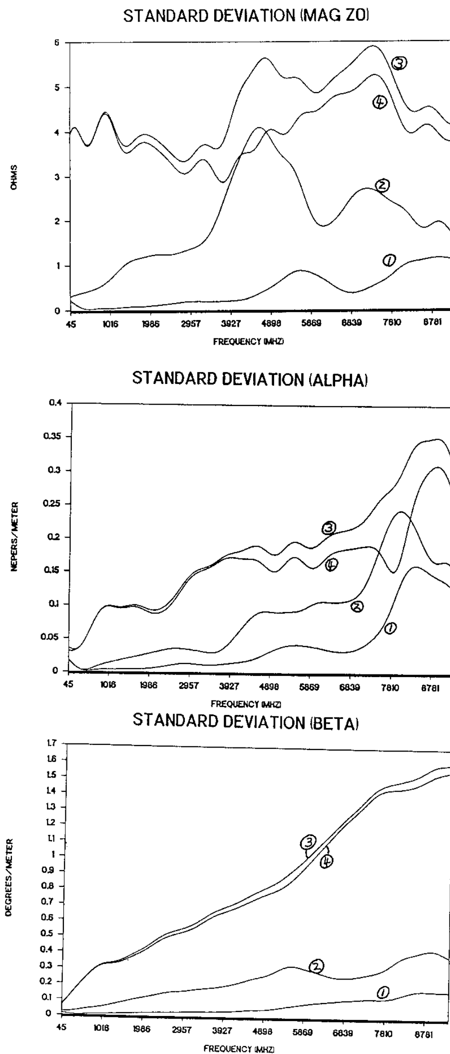


An important result is the repeatability of the aspects of this measuring technique. Even though a torque wrench is used, connecting the ANA to the SMA causes measurable random deviation. Soldering connectors will cause significant errors even at relatively low frequencies. Therefore, it is important to take these effects into consideration when using this measuring technique in the analysis of the measured data.

## Conclusion

The lack of sufficient repeatability in PCB manufacturing can cause inaccurate simulation of high-speed digital circuits. One solution to this problem is to characterize the deviation so that a worst case analysis can be performed. This is accomplished by measuring a number of structures and generating the characteristic impedance and propagation constant for each structure. These two parameters are used in the statistical modeling of PCB lines and discontinuities. If the circuit performs properly under the worst possible conditions, the designers can be confident that they will have fewer post-prototype problems.

## Reference


[1] Riedell, Heyward, Kay, M., Steer, M., Basil, M., and Pomerleau, R. 'Dielectric Characterization of Printed Circuit Substrates', Proceedings IEEE Southeast Con 89.

[2] Kasten, J., Steer,, M., and Pomerleau, R. 'Through Symmetric Fixture: A Two-Port S-Parameter Calibration Technique', Proceedings RF Expo East 88.

[3] Menden, Schaeffer, and Wackerly. Mathematical Statistics with Applications. 3rd ed Duxbury, 1986.

# Field Behavior Near Surface Discontinuities Of The Gyrotropic Medium

Benjamin Beker
University of South Carolina
Columbia, South Carolina

Korada R. Umashankar
University of Illinois
Chicago, Illinois

## Abstract

The local electromagnetic field behavior in the vicinity of wedge-like homogeneous, gyrotropically anisotropic, structures is considered. The theoretical analysis is based on the static theory involving a rigorous solution of the field boundary-value problem leading to a transcendental equation explicitly dependent on the gyrotropic medium parameters, as well as the opening angle of the wedge. The numerical solution to this equation is obtained for the power to which the radial distance governing the electromagnetic field behavior close to the surface discontinuity is raised, and results for some gyrotropic media are presented.

## Introduction

In recent years the use of anisotropic, particularly gyrotropic, materials has found its way into applications dealing with substrates for microwave integrated circuits, microstrip antennas, and electromagnetic scattering from objects having complex geometrical shapes. In all of the above applications the problem very often involves discontinuous material boundaries in the form of sharp corners or bends. These surface discontinuities are mostly responsible for altering the electromagnetic field distribution in the vicinity of the wedge-like geometrical regions of the material boundary. As opposed to the case of a perfectly conducting or even a dielectric wedge, the exact nature of field distribution in the localized region near the tip of the anisotropic wedge is still unknown. In this paper the study of electromagnetic field distribution near a sharp surface discontinuity of a homogeneous gyrotropically anisotropic medium will be considered. The formulation will be based on the static theory and the appropriate boundary-value problem will be solved to determine an appropriate transcendental equation whose numerical solution will be shown to contain the desired information indicative of the field characteristics near such localized regions. The static approach leads to accurate results even for the dynamic case whenever the radial distance from the surface discontinuity to the observation point remains small compared to the wavelength of the electromagnetic field.

## Theory

Consider a two-dimensional gyrotropic wedge having an opening angle $2\varphi_o$ and characterized by a second rank tensor, $\varepsilon$, (a 3X3 square matrix) with the following parameters:

$$\varepsilon_{xx} = \varepsilon_{yy} = \varepsilon_1 \,, \quad \varepsilon_{zz} = \varepsilon_2$$

$$\varepsilon_{xz} = \varepsilon_{zx} = \varepsilon_{yz} = \varepsilon_{zy} = 0$$

$$\varepsilon_{xy} = -\varepsilon_{yx} = j\varepsilon_3 .$$

Furthermore, let the electrostatic potential inside the gyrotropic medium be denoted by $\Phi_1$ and correspondingly the potential in the surrounding ambient medium by $\Phi_2$, both of which are assumed to satisfy the scalar Laplace equation in their respective regions of validity, i. e.,

$$\nabla 2\, \Phi_2 = 0 \qquad \varphi_o < \varphi < 2\pi - \varphi_o \tag{1}$$

$$\nabla\cdot(\varepsilon\cdot\nabla\Phi_1) = 0 \quad -\varphi_o < \varphi < \varphi_o \tag{2}$$

where $\varepsilon$ is the gyrotropic medium tensor whose elements have been specified above. Near the tip of the wedge the power series solution to the Laplace equation in each angular sector occupied by different media may be accurately approximated by the first term only. Hence, the final form of the solution for (1) and (2) may be written as:

$$\Phi_2=\rho^{\nu}\{A \cos(\nu(\pi-\varphi)) + B \sin(\nu(\pi-\varphi))\}=\Phi^e{}_2 + \Phi^o{}_2 \tag{3}$$

$$\Phi_1=\rho^{\nu}\{C \cos(\nu\varphi) + D \sin(\nu\varphi)\}=\Phi^e{}_1 + \Phi^o{}_1 \tag{4}$$

where the $\Phi^o$ and $\Phi^e$ denote the odd and even parts of the potential, respectively, and the corresponding electric flux density in the two regions of space can be shown to have the following form:

$$\mathbf{D}_2 = -\varepsilon_o \nabla\Phi_2 \tag{5}$$

$$\mathbf{D}_1 = -\varepsilon \cdot \nabla\Phi_1 \tag{6}$$

The remaining portion of the analysis is carried out employing the procedure used earlier for the isotropic dielectric and permeable media[1]. This approach involves seeking the solution to the odd and even parts of (3) and (4) independently and then obtaining the total solution by superposition. In the following only the solution for the even part of the potential is considered in detail, because the analytic form for the corresponding odd portion, $\Phi^o$, may simply be found by taking analogous steps used in determining $\Phi^e$.

In order to obtain a transcendental equation for $\nu$ which governs the radial dependence of the static potential as well as the electric field, it is necessary to enforce the appropriate

CH2674-5/89/0000-0117$01.00©1989IEEE

boundary conditions at $\varphi = \varphi_o$. These conditions state that the potential itself must be continuous across the material boundary in addition to the continuity of its normal derivative, in this case $\partial/\partial\varphi$, scaled by the corresponding medium parameters (or equivalently $\mathbf{D}_\varphi$) on each side of the boundary. Enforcing above requirements on $\Phi^e$ and performing the necessary abgebraic manipulations leads to the desired equation which contains all of the required information regarding the material parameters and the wedge opening angle, i.e.,

$$\varepsilon_1 \tan(\nu\varphi_o) + j\varepsilon_3 = - \varepsilon_o \tan(\nu(\pi - \varphi_o)) \qquad (7)$$

where $\varepsilon_o$ is the permittivity of free-space. Once the solution to (7) for the unknown parameter $\nu$ is determined, it becomes possible to establish the exact nature of the electric field variation in the vicinity of the tip of the wedge, that is, in the region of $\rho \to 0$. This turns out to be a direct consequence of the $\rho$ dependence of the field which due to the even portion of the potential is equal to

$$\mathbf{D}^e_2 = - \varepsilon_o \cos(\nu\varphi_o)\, C\, \nu\rho^{(\nu-1)}\{\mathbf{a}_\rho \cos(\nu(\pi - \varphi))$$

$$+ \mathbf{a}_\varphi \sin(\nu(\pi - \varphi))\}/\{\cos(\nu(\pi - \varphi_o))\} \qquad (8)$$

$$\mathbf{D}^e_1 = C\, \nu\rho^{(\nu-1)}\{-\mathbf{a}_\rho(\varepsilon_1 \cos(\nu\varphi) - j\varepsilon_3 \sin(\nu\varphi))$$

$$+ \mathbf{a}_\varphi(\varepsilon_1 \sin(\nu\varphi) + j\varepsilon_3 \cos(\nu\varphi))\} \qquad (9)$$

where $\mathbf{a}_\rho$ and $\mathbf{a}_\varphi$ are the cylindrical $\rho$ and $\varphi$ unit vectors. Therefore, if the value of $\nu$ is less that one, the field becomes singular whenever the observation point moves towards the tip of the gyrotropic wedge. If on the other hand the root of (7) turns out be greater that one, the magnitude of the electric flux density tends towards zero as the field point approaches the surface discontinuity.

Similarly, the transcendental equation for $\nu$ due to the odd part of $\Phi$ may be obtained following the steps taken to derive (7), and specifically for this case it turns out to have the following form:

$$\varepsilon_1 \cot(\nu\varphi_o) - j\varepsilon_3 = - \varepsilon_o \cot(\nu(\pi - \varphi_o)) \qquad (10).$$

The explicit expressions for the field may now be determined from equations (5) and (6) inside as well as outside the anisotropic material wedge.

Finally, it should be pointed out that a dual case, i. e. one involving a permeable gyrotropic medium often referred to as Ferrite, may be analyzed via duality. This simply implies that the magnetostatic scalar potential $\Psi$ will be required to determine the magnetic flux density $\mathbf{B}$ for the wedge material characterized by a tensor $\mu$.

## Numerical Results

Consider a gyrotropic material wedge whose constitutive tensor elements are $\varepsilon_1 = 2.5$, $\varepsilon_3 = 2.0$, and its half-opening angle $\varphi_o$ is equal to $\pi/4$. The value of $\nu$ characterizing the behavior of the electric field due to the even mode of the static potential, $\Phi^e$, near the tip of the wedge may be numerically calculated from equation (7) which may have more than one solution. In this case the smallest positive value of $\nu$ must be retained for it is solely responsible for determining the upper bound of the field singularity. Since the transcendental equation is complex, its roots are expected to be complex as well. And in fact, this indeed turns out to be the case, i.e, $\nu = (0.79852 + j0.11026)$. Therefore, the field whose radial part is then raised to the power of $\rho^{(-0.20148 + j0.11026)}$ clearly exhibits singular properties as $\rho \to 0$. As a second example consider same parameters as above, but with the exception of $\varepsilon_3$ which is now assumed to be -2.0. The numerically computed root of (7) will now become a complex conjugate of that calculated previously. This, of course is not at all surprizing because the medium tensor, as well as equation (7), become complex conjugates of those considered before. Next, if the off-diagonal element $\varepsilon_3$ is taken to be j2.0, then (7) is purely real and its root, $\nu$, is now 0.37787. The power of $\rho$ characteristic to this medium becomes equal to -0.62213, and form equations (8) and (9) it is clearly obvious that the field near the tip of the wedge is indeed singular.

Next, consider the contribution to the overall electric field in the region close to the tip resulting from $\Phi^o$. The power $\nu$ for this mode can be determined from equation (10). Once again using the medium parameters and the wedge half-opening angle identical to those employed in computations dealing with the even mode, the roots for this case have been calculated and are displayed bellow:

$\varepsilon_3 = 2.0 \qquad \nu = (1.2015 + j0.11026)$

$\varepsilon_3 = -2.0 \qquad \nu = (1.2015 - j0.11026)$

$\varepsilon_3 = j2.0 \qquad \nu = (2.3778 + j0.00000)$

where of course $\varepsilon_1 = 2.5$ and $\varphi_o = \pi/4$. The above listed roots, $\nu$, all have real parts greater that unity, thereby implying that the odd part of the static potential will not contribute to the singular behavior of the field.

## Conclusion

In this paper the field behavior characteristic to the gyrotropically anisotropic homogeneous medium has been examined. It was found that much in the same manner as for the isotropic dielectric or permeable material and wedge-like geometries the electromagnetic field exhibits singular properties in the vicinity of surface discontinuities. This conclusion is based on the numerical solution of the analytically derived transcendental equation whose roots, depending on the medium as well as the geometrical parameters, lead to the appropriate power governing the radial and subsequently the singular behavior of the field. It has also been explicitly shown which of the two possible modes (odd or even) of the static potential is responsible for the singular characteristics of the electromagnetic field.

## Reference

[1] J. Van Bladel, "*Field Singularities at Metal-Dielectric Wedges*", IEEE Trans. on Antennas and Prop., vol. AP-33, no. 4, pp. 450-454, Apr. 1985.